Check for updates

How to cite:
International Edition: doi.org/10.1002/anie.202016185
German Edition: doi.org/10.1002/ange.202016185

Double Perovskites

Doubling the Stakes: The Promise of Halide Double Perovskites

*Nathan R. Wolf[+], Bridget A. Connor[+], Adam H. Slavney, and Hemamala I. Karunadasa**

Keywords:
band structure · double perovskites · perovskites · photovoltaics · semiconductors

Dedicated to Prof. Harry B. Gray on the occasion of his 85th birthday

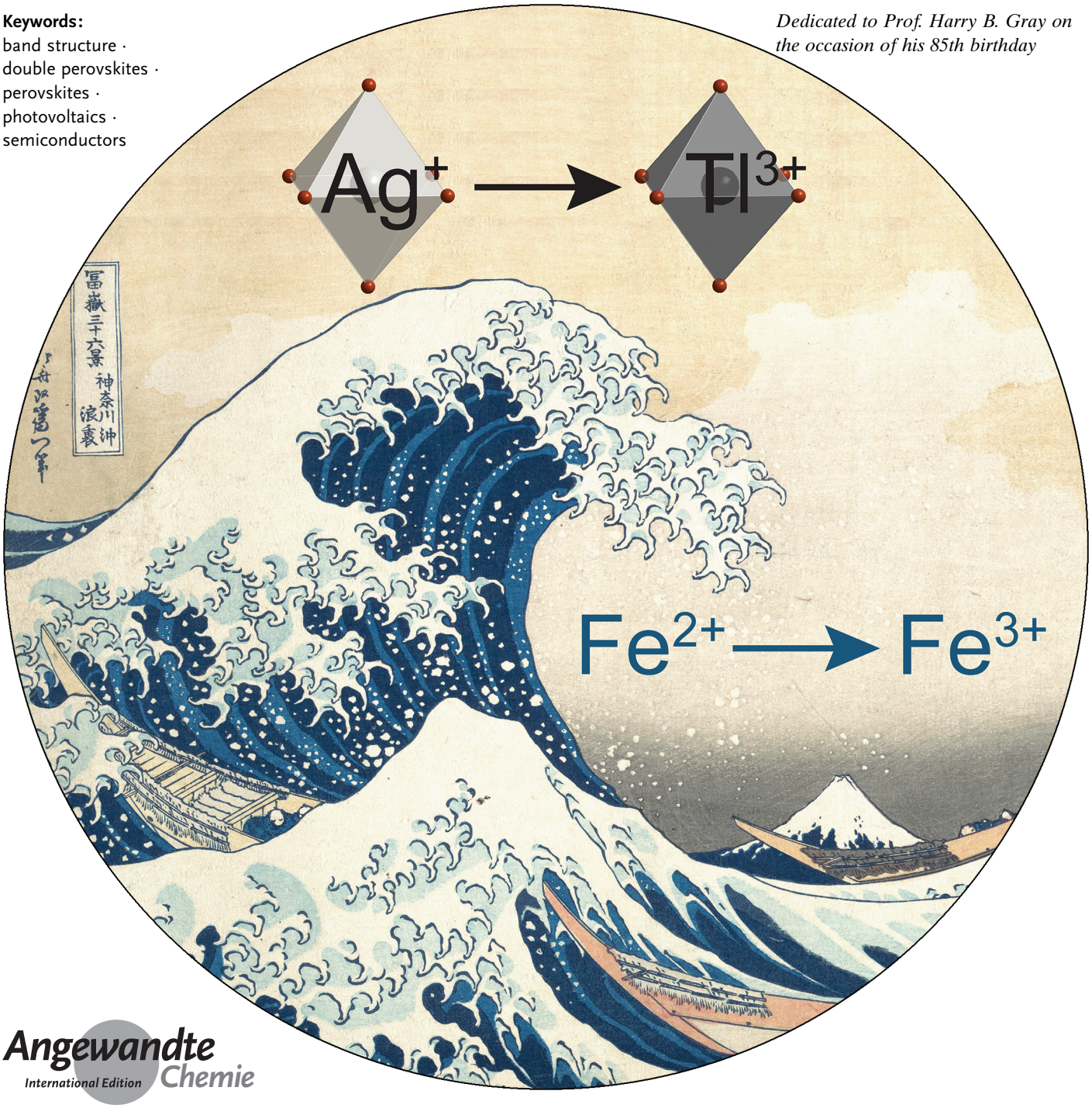

© 2021 Wiley-VCH GmbH

These are not the final page numbers!

When the stakes are doubled in a wager, a player must correctly place two consecutive bets to win, but the payout is larger. Similarly, two B sites in combination dictate the properties of $A_2BB'X_6$ (A = monocation, X = halide) double perovskites. Correctly picking two B sites is more challenging than picking just one, as in the $A^IB^{II}X_3$ single perovskites, but the options are greater and, we believe, the rewards are higher when the stakes are doubled. In this Minireview, we emphasize fundamental aspects of halide double perovskites to provide a foundation for interested readers to explore this extraordinary class of materials. In particular, we highlight the differences and similarities between double and single perovskites and describe how the double perovskite structure potentially offers greater control over photophysical properties.

1. Introduction

Halide perovskites, which date back to the 1800s,[1] are crystalline semiconductors formed in solution-state or mild solid-state reactions. These ionic solids consist of anionic metal-halide octahedra connected in 0, 1, 2, or 3 dimensions through shared corners, with inorganic or organic cations providing charge compensation. Research efforts on three-dimensional (3D) lead-halide perovskites have recently been invigorated due to the remarkable rise in the efficiencies of solar cells employing these materials as absorbers, specifically, $(MA)PbI_3$ ($MA = CH_3NH_3^+$)[2] and its derivatives.[3] However, lead perovskites constitute only a small section of the vast and diverse family of halide perovskites. Thus, more recently, researchers have sought to cast a wider net in search of new compositions that mimic the optoelectronic properties of the lead perovskites.[4] These efforts seek to both understand the origin of the remarkable optoelectronic properties of lead perovskites through fundamental studies and to identify functional analogues with improved stability as well as reduced toxicity and environmental impact.[4a] Of all the alternatives that have been explored, the $A_2BB'X_6$ (A = monocation, X = halide) double perovskites have emerged as the most abundant and promising family.[5] Double perovskites maintain a similar structural framework to that found in single perovskites while permitting a wider variety of cations to be incorporated into the octahedrally coordinated B/B′ site. This enables access to an expansive range of alternative compositions and electronic structures, which researchers are only beginning to explore.

Herein, we discuss select structural and optoelectronic topics relevant to contemporary research on halide double perovskites. This Minireview will not address nanostructuring[6] nor detail device applications,[7] except for a brief discussion of the latter in the concluding section. In Section 1, we define double perovskites and briefly survey their history. Section 2 discusses different subclasses of double perovskites, including their two-dimensional (2D) variants and the local structural distortions that occur in these materials. Section 3 gives an overview of double perovskite electronic structures and highlights simple rules that predict the electronic structures of undiscovered compounds. In Section 4, we detail strategies for modifying the electronic structure. We conclude in Section 5 by emphasizing commonalities between double perovskites and other well-known materials families, which we hope will provide direction for future studies.

1.1. Definition of 3D Double Perovskites

As a materials family with a long, rich history, double perovskites have acquired various definitions, which are the subject of continuing discussion.[8] For the purposes of this Minireview, we follow a relatively restrictive definition of 3D halide double perovskites by including only materials that meet the following criteria:

1. The structure contains cations or vacancies surrounded by six halides ($[BX_6]^{n-}$; B = cation or vacancy; X = halide).
2. The $[BX_6]^{n-}$ units are exclusively corner-sharing in a 3D pattern (B = cation or vacancy; X = halide).
3. There are exactly two structurally distinguishable $[BX_6]^{n-}$ motifs in the unit cell, such that the chemical formula must be $A_2BB'X_6$ (B = cation or vacancy; X = halide).

The third criterion, requiring exactly two distinct $[BX_6]^{n-}$ units, distinguishes double perovskites from single perovskites (Figure 1). The ordering of these distinct $[BX_6]^{n-}$ units significantly impacts the material's electronic structure (see Section 3).[9] Fully disordered alloys with only one distinct B site, such as $A(Pb_{1-x}Sn_x)X_3$ (which were investigated as early as the 1970s[10] and recently used in solar cells[11]) are thus classified as single perovskites. In the oxide literature, materials with two distinct, ordered A sites ($AA'B_2X_6$) are commonly considered double perovskites.[12] We exclude such compositions from our definition because examples of A-site ordered halide perovskites are extremely rare[13] and because such materials are expected to exhibit optoelectronic properties more similar to those of single perovskites (see Section 3.1).

[*] N. R. Wolf,[+] Dr. B. A. Connor,[+] Dr. A. H. Slavney, Prof. H. I. Karunadasa
Department of Chemistry, Stanford University
Stanford, California 94305 (USA)
Prof. H. I. Karunadasa
Stanford Institute for Materials and Energy Sciences
SLAC National Accelerator Laboratory
Menlo Park, California 94025 (USA)
E-mail: hemamala@stanford.edu
[+] These authors contributed equally to this work.
The ORCID identification numbers for the authors of this article can be found under: https://doi.org/10.1002/anie.202016185.

 © 2021 Wiley-VCH GmbH

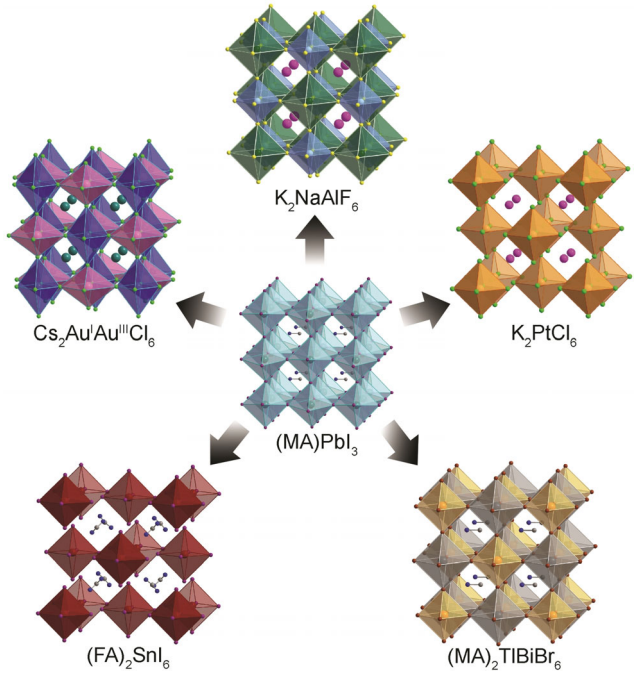

Figure 1. A sample of known double perovskite structures demonstrating the structural and compositional diversity of this family. From the top proceeding clockwise, the crystal structures of: K_2NaAlF_6,[22] K_2PtCl_6,[19] $(MA)_2TlBiBr_6$ (MA = methylammonium),[56] $(FA)_2SnI_6$ (FA = formamidinium),[83c] and $Cs_2Au^IAu^{III}Cl_6$.[23] The single perovskite $(MA)PbI_3$[11a] is shown in the middle. Atom colors: dark green = Na, light blue = Al, dark orange = Pt, light-orange = Bi, black = Tl, dark red = Sn, dark blue = Au^{III}, light pink = Au^I, turquoise = Pb, magenta = K, teal = Cs, purple = I, brown = Br, green = Cl, yellow = F, gray = C, and blue = N; H atoms are omitted.

1.2. Double Perovskite Nomenclature

Although the term "double perovskite" conveniently includes all halide perovskites with distinct B and B′ sites, historically the $A_2B^IB^{III}X_6$ and the $A_2B^{IV}\square X_6$ (□ = vacancy) perovskites have been considered as separate families. In the older literature, the $A_2B^IB^{III}X_6$ compounds are known as elpasolites after the mineral elpasolite, K_2NaAlF_6.[1a,14] The $A_2B^{IV}\square X_6$ perovskites have been known by many names over the decades, including double halides,[15] complex antifluorites,[16] hexahalogenometallates,[17] and, most recently, vacancy-ordered double perovskites.[18] Here, we refer to these materials as "K_2PtCl_6-type perovskites" after one of the early $A_2B^{IV}\square X_6$ compounds to be structurally characterized.[19] In the following sections, we give a brief overview of the historical development of these two subdivisions of double perovskites, highlighting important bodies of work and key milestones in Figure 2.

1.3. History of Elpasolites

Elpasolites have been known since the late 19th century[1a,14] and predate the development of X-ray diffraction. The earliest report appears to be the 1883 discovery of the mineral elpasolite, K_2NaAlF_6, identified by the distinctive 2:1:1:6 ratio in the elemental analysis of rock samples near Pikes Peak in El Paso County, Colorado, USA.[1a] The first reported synthesis of an elpasolite was of $Cs_2Au^IAu^{III}Cl_6$ in 1922.[20] The early application of X-ray crystallography revealed the atomic structure of K_2NaAlF_6 in 1932,[21] although the space group was incorrectly assigned,[22] and the structures of $Cs_2Au^IAu^{III}Cl_6$ and $Cs_2Ag^IAu^{III}Cl_6$ in 1938 (Figure 1).[23] Until the 1970s, additional studies on elpasolites were largely

Nathan Wolf received his A.B. in 2016 from Washington University in St. Louis, where he studied chemistry and French while researching protein biochemistry. He is now carrying out Ph.D. research with Prof. H. I. Karunadasa at Stanford University on metal halide materials at high pressures and investigating electronic interactions across vacancies with a view to renewable energy technologies.

Adam Slavney received his A.B. in Chemistry in 2014 from Washington University in St. Louis and his Ph.D. in 2019 from Stanford University with Prof. H. I. Karunadasa, where he studied halide double perovskites. He is currently an Arnold O. Beckman Postdoctoral Fellow in the group of Prof. J. A. Mason at Harvard University.

Bridget Connor received her B.S. in Chemistry in 2015 from Caltech, where she conducted research with Prof. J. C. Peters on small-molecule activation by first-row transition-metal complexes. In her Ph.D. work at Stanford University with Prof. H. I. Karunadasa, she explored the effects of electronic confinement on halide double perovskites by synthesizing and characterizing 2D analogues.

Hemamala Karunadasa studied solid-state chemistry with Prof. R. J. Cava for her A.B. from Princeton University. She received her Ph.D. in 2009 from UC Berkeley. She studied molecular coordination complexes with Profs. J. R. Long and C. J. Chang at Berkeley and with Prof. H. B. Gray at Caltech. She is an Associate Professor of Chemistry at Stanford University and a Principal Investigator at the SLAC National Lab. Her group bridges the chemistry of molecules and extended solids.

© 2021 Wiley-VCH GmbH

These are not the final page numbers!

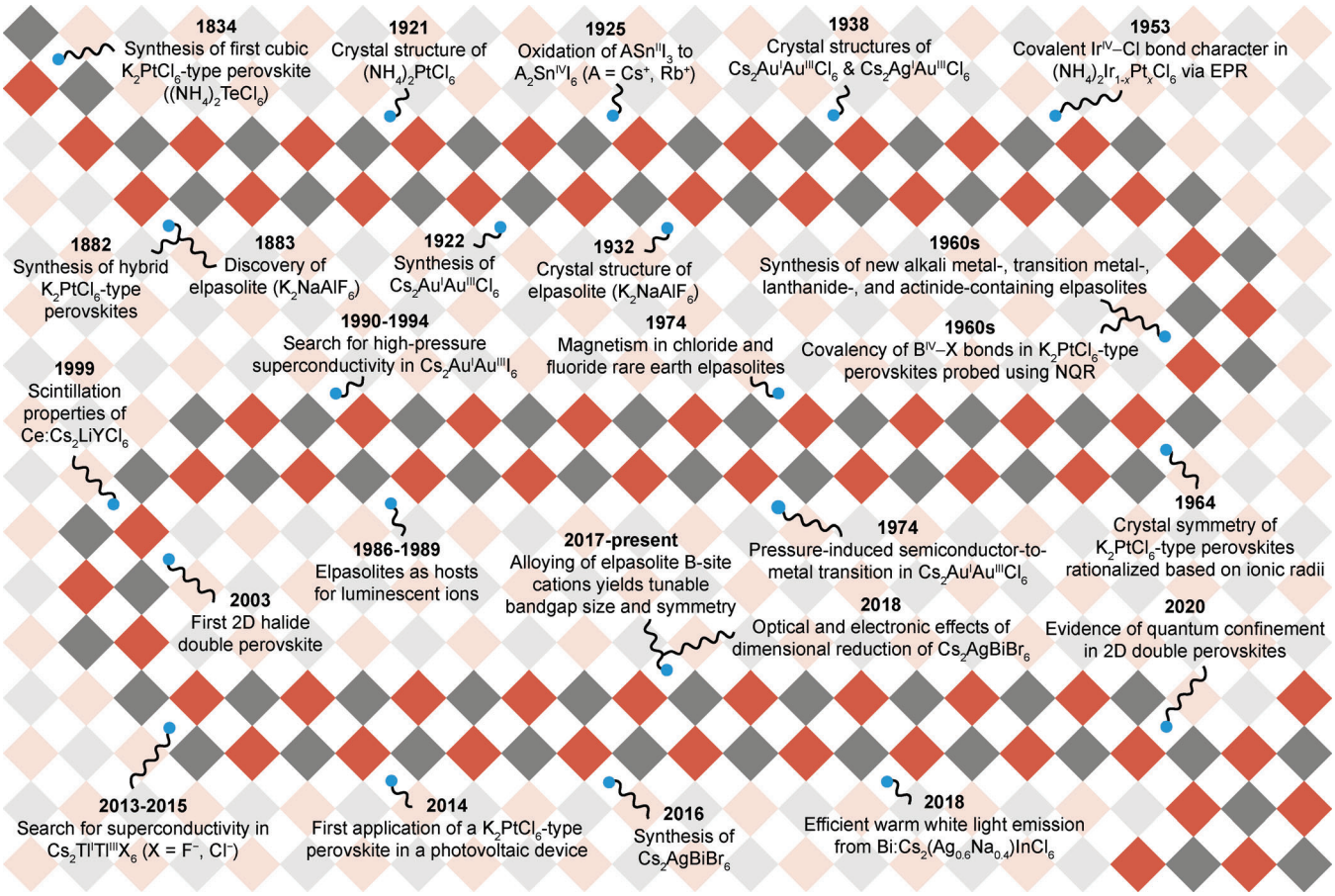

Figure 2. Timeline of important milestones and events in the development of elpasolites and K_2PtCl_6-type perovskites.

structural,[24] greatly increasing the number of known materials, particularly those containing lanthanides (Figure 3).[25] One vein of work, beginning in the 1970s, exploited the local octahedral site symmetry of elpasolites to study the magnetic and electronic properties of lanthanide-based structures[26]

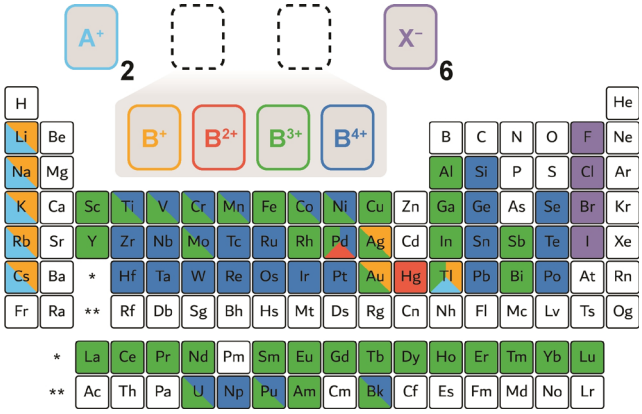

Figure 3. The compositional diversity of 3D halide double perovskites spans the majority of the periodic table. Light blue, orange, red, green, blue, and purple signify an element's reported stoichiometric incorporation in a 3D halide double perovskite as A^+, B^+, B^{2+}, B^{3+}, B^{4+}, and X^-, respectively. Double perovskites with alloyed or mixed B sites are not included here.

and to form luminescent materials through lanthanide or transition-metal doping.[27] Meanwhile, a separate body of work spanning more than 50 years explored mixed valency in elpasolites. Beginning in the 1950s, elpasolites with the general formula $Cs_2BAu^{III}X_6$ (B = Ag^I, Au^I, X = Cl^-, Br^-, I^-) were investigated as part of the widespread interest in mixed valency at the time.[28] These early studies laid the groundwork for experiments throughout the 1970s and 1980s, which probed how high pressure influences the structural and mixed-valence electronic properties of these materials.[29] In the 1990s, $Cs_2Au^IAu^{III}I_6$ gained renewed interest after the discovery of superconductivity in $(Ba_{1-x}K_x)_2Bi^{III}Bi^VO_6$, another mixed-valence double perovskite.[30] Although a semiconductor-to-metal transition was observed in $Cs_2Au^IAu^{III}I_6$ at high pressures,[31] attributed to the comproportionation of Au^I and Au^{III} to Au^{II},[32] no superconductivity has yet been observed. Nevertheless, the search for superconductivity in mixed-valence double perovskites continues, with more recent studies investigating $Cs_2Tl^ITl^{III}X_6$ (X = F^-, Cl^-).[33] The mixed-valence Au^I-Au^{III} elpasolites returned to the scene in 2003 when Guloy and co-workers reported the first example of a 2D elpasolite $(A)_2[(Au^II_2)(Au^{III}I_4)(I_3)_2]$ (A = 1,8-octanediammonium or 1,7-heptanediammonium),[34] where the 3D structure of $Cs_2Au^IAu^{III}I_6$ is thinned to a single sheet of corner-sharing octahedra (see Section 2.4), albeit with some terminal I^- ligands replaced by I_3^- ligands.[35]

© 2021 Wiley-VCH GmbH

1.4. History of K_2PtCl_6-Type Perovskites

The origin of K_2PtCl_6-type perovskites dates back to the synthesis of A_2TeX_6 ($A = K^+$, Na^+, NH_4^+ and $X = Cl^-$, Br^-, I^-) in 1834.[36] Before the 1920s, studies focused on synthesis, elemental analysis, and crystal morphology.[15,37] Large organic cations were commonly employed as A-site cations, thus demonstrating the close association of K_2PtCl_6-type perovskites with molecular salts.[37b,d,38] A series of X-ray crystallographic studies in the 1920s showed that these materials consist of isolated octahedra (Figure 1).[19,39] The authors immediately recognized the similarity to the CaF_2 fluorite structure, where $PtCl_6^{2-}$ replaces Ca^{2+} and K^+ replaces F^- (Figure 4 A,B), thereby leading to their classification as antifluorites. Many more K_2PtCl_6-type perovskites were subsequently characterized,[40] and at least 30 elements have been incorporated at the B site to date (Figure 3).[41] A number of these materials exhibit symmetry-lowering octahedral rotations as a result of over- or undersized A-site cations (see Section 2.5.2).[42] A structural analysis, similar to the Goldschmidt tolerance factor,[43] was first developed in 1964 by Brown, which enabled prediction of cubic K_2PtCl_6-type perovskites and rationalized their temperature-dependent phase-change behavior.[42,44] The rapid diversification of the K_2PtCl_6-type perovskites led to a growing interest in their fundamental properties. Throughout the 1960s, these materials were used to investigate the covalency of the metal-halide bond of $[BX_6]^{2-}$ octahedral complexes (particularly for B = third-row transition metal) using pure quadrupole resonance spectroscopy.[45] Additionally, much like elpasolites, K_2PtCl_6-type perovskites were found to be excellent host structures for metal alloying, facilitating the discovery of covalent π-bonding in $IrCl_6^{2-}$ by electron paramagnetic resonance spectroscopy,[46] charge transfer between mixed-valence Sb^{III} and Sb^{V} ions by optical spectroscopy,[47] and photon upconversion from Re^{4+} ions doped into a Cs_2ZrCl_6 host structure.[27d,48]

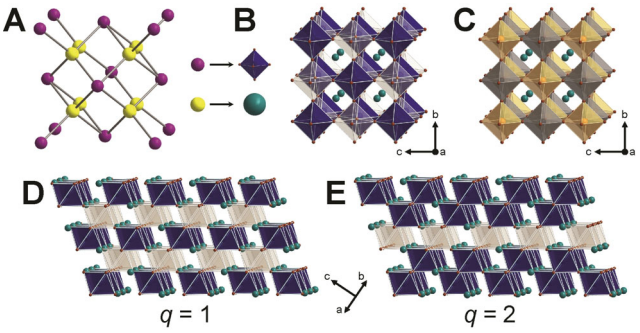

Figure 4. The K_2PtCl_6-type structure (B) can be derived from the structure of CaF_2 (A) by replacing Ca^{2+} (purple spheres) with $PtCl_6^{2-}$ (blue octahedra) and F^- (yellow spheres) with K^+ (turquoise spheres) or from the elpasolite structure (C) by replacing one of the B-site cations with a vacancy (transparent octahedra). This structure type is also a member of the $q = 1$ (111) family of perovskites, derived by removing all B sites lying along every other (111) crystallographic plane (D). The $q = 2$ members of this (111) family (E), where every third (111) plane of B sites is removed, do not meet our definition of a double perovskite (see Section 1.1).

1.5. Recent Work

The recent revival of interest in halide double perovskites originates from the search for nontoxic alternatives to $APb^{II}X_3$ in perovskite photovoltaics.[4a] The first comments on the K_2PtCl_6-type perovskites in recent perovskite literature arose from the known[49] undesired oxidation of $ASn^{II}I_3$ to $A_2Sn^{IV}I_6$,[11a,50] followed by a 2014 investigation of Cs_2SnI_6 for photovoltaic applications.[7b] The following year, a computational paper proposed the hypothetical elpasolite $(MA)_2TlBiI_6$ as a potential photovoltaic absorber.[51] This early work did not refer to the subject materials as double perovskites. Recognition of the potential of the halide double perovskite family as a whole arrived in 2016, when three groups independently reported the synthesis and optoelectronic properties of the elpasolites Cs_2AgBiX_6 ($X = Cl^-$ and/or Br^-).[52] Since then, many new elpasolites have been synthesized, including $Cs_2AgInCl_6$,[53] Cs_2AgTlX_6 ($X = Cl^-$, Br^-),[54] $Cs_2AgSbCl_6$,[55] $(MA)_2TlBiBr_6$,[56] and various alloys.[55,57] This recent growth of novel elpasolite compositions has sparked an interest in many K_2PtCl_6-type perovskites well-known in the early literature, such as Cs_2TeI_6,[15] Cs_2PdBr_6,[37c] Cs_2SnI_6,[58] Cs_2PtI_6,[59] and Cs_2TiI_6,[60] as researchers reinvestigate these materials in the context of photovoltaics.[18,61] The recent interest in halide double perovskites as photovoltaic absorbers has led to new applications for these materials[7] while also serving as a platform for more fundamental studies, such as investigations into the consequences of dimensional reduction.[62] In particular, a recent flurry of reports has increased the phase space of 2D elpasolites, starting with Ag-Bi in 2018[62a] and then expanding to Ag-Tl,[62b] Ag-In,[62c] and Cu-Bi.[62d] The young, but rapidly growing, field of lower-dimensional double perovskites is likely to greatly expand the structural and functional diversity of the double perovskite family in the coming years, as witnessed previously for the halide single perovskites.[63]

2. A Structural Survey

In the following sections, we discuss some of the most important aspects of the double perovskite structure, including B-site ordering, dimensional reduction, and structural distortion.

2.1. Thermodynamics of B-Site Ordering

B-site ordering distinguishes double perovskites from single perovskites. In halide double perovskites, this ordering is thermodynamically favored. For example, the complete disordering of the Ag^+ and Bi^{3+} cations in $Cs_2AgBiBr_6$ is calculated to occur only above 3000 K.[64] At room temperature, entropically driven B-site disordering is likely present but only at such low levels that it is better discussed as a propensity for the formation of anti-site defects.[65] Similar to the case of the oxide perovskites, B-site ordering is likely driven by electrostatics, as having adjacent 3+ or 4+ cations is unfavorable.[8a,b] Indeed, isovalent B and B′ cations most

© 2021 Wiley-VCH GmbH

These are not the final page numbers!

commonly form disordered single perovskites (e.g. $A(Sn_{1-x}Pb_x)X_3$).[10] One notable exception is $Cs_2Hg^{II}Pd^{II}Cl_6$, where octahedral distortions drive B-site ordering.[66] Likewise, in alloying studies, the speciation of the impurity cation in the host double perovskite depends strongly on its charge, generally resulting in isovalent substitution (see Section 4.1).[7a,18,55,57a,b]

2.2. B-Site Ordering Motifs

All known halide double perovskites display rock-salt ordering. Here, each $[BX_6]^{n-}$ unit is surrounded by six $[B'X_6]^{m-}$ units and vice versa, thereby forming a 3D checkerboard pattern reminiscent of the ordering of Na^+ and Cl^- ions in the NaCl rock-salt structure. Intriguingly, octahedral distortions stabilize several more exotic forms of B-site ordering in the oxide perovskites,[67] including layered[68] and columnar arrangements.[8a,b,67] Such orderings may also be possible in the halides, although, to date, all halide double perovskites with highly distorted $[BX_6]^{n-}$ units display rock-salt ordering.[23,66]

2.3. Stoichiometric Vacancies

The K_2PtCl_6-type perovskite structure is equivalent to the elpasolite structure where one of the B sites is a vacancy (Figure 4B,C). Alternatively, the K_2PtCl_6-type perovskite structure can be viewed according to the definition of (111) perovskites set forth by Mitzi.[69] This perovskite family is derived from the single perovskite structure by slicing along a series of evenly spaced (111) crystallographic planes, effectively generating planes of B-site vacancies (Figure 4D). The index q refers to the number of metal halide layers lying between planes of vacancies. Although halide perovskites with $q = 1$, 2, and 3 have been reported,[63a,69,70] those with $q = 2$ (Figure 4E) and 3 do not fit our definition of double perovskites (see Section 1.1) or dimensionally reduced double perovskites (see Section 2.4). Only the $q = 1$ structure, where half of the B sites are replaced by vacancies, qualifies as a double perovskite.

2.4. Dimensional Reduction

Despite the extensive history of halide double perovskites, their lower-dimensional derivatives remained completely unexplored until relatively recently.[34,62a] We define lower-dimensional halide double perovskites as materials whose inorganic framework can be derived through dimensional reduction[71] of a 3D double perovskite (which, according to our definition in Section 1.1, requires an ordered arrangement of two distinct $[BX_6]^{n-}$ units). Whereas a structurally diverse array of lower-dimensional halide single perovskites exists,[69] such variety has not yet been achieved for halide double perovskites. In the following sections, we highlight the known structure types of layered double perovskites and identify missing topologies to motivate continued exploration.

2.4.1. The (001) Perovskites

To date, all examples of dimensionally reduced double perovskites[34,62a–d,72] belong to the (001) elpasolite family, where the inorganic framework is derived from a slice taken along the (001) crystallographic plane of the $A_2BB'X_6$ structure (Figure 5A).[69] This 2D perovskite structure consists of flat sheets of corner-sharing, alternating $[BX_6]^{n-}$ and $[B'X_6]^{m-}$ octahedra. These sheets can consist of one or multiple layers of stacked octahedra (Figure 5A). Thicker slabs require a specific ratio of small and large A-site cations. The larger A′ monocations partition the 3D structure into sheets, while the smaller A cations occupy cuboctahedral cavities within the sheets, thereby yielding the general formula $A'_4A_{2n-2}B_nB'_nX_{6n+2}$, where n is the number of octahedral layers forming the inorganic slabs. Unlike in the tin- and lead-based materials, where layered perovskites with $1 \le n \le 7$ have been crystallographically characterized,[73] thus far, only $n = 1$ and 2 members of the (001) elpasolites are known.[34,62a–c] Note that we have restricted our list of 2D double perovskites to those with demonstrated crystallographic B-site ordering. Nevertheless, there are several reports of 2D double perovskites with disordered 1+ and 3+ B-site cations, although it is so far unclear whether this disorder arises solely from a lack of registry between adjacent

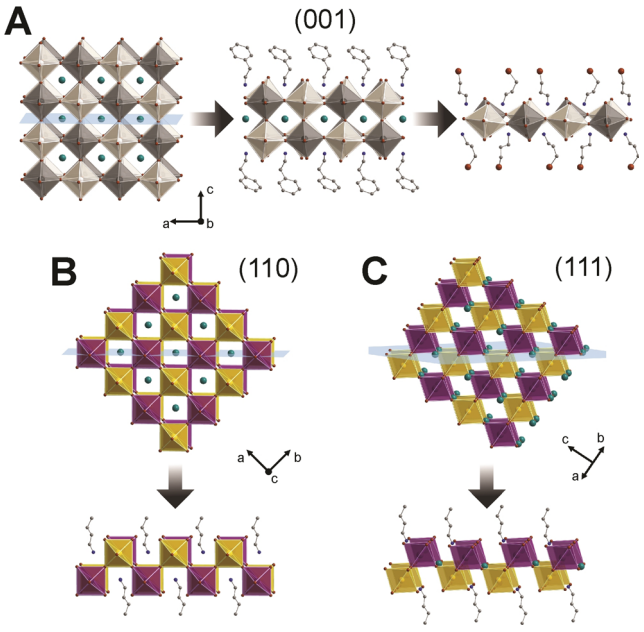

Figure 5. Dimensional reduction of the 3D double perovskite framework to yield 2D double perovskites with different topologies. All known examples of lower-dimensional halide double perovskites belong to the (001) family (A); inorganic slabs with bilayer ($n = 2$) and monolayer ($n = 1$) thicknesses have been prepared. Pictured here from left to right are the single-crystal X-ray structures of 3D $Cs_2AgTlBr_6$[54] and its $n = 2$ and $n = 1$ derivatives.[62b] Black, white, brown, teal, blue, and gray spheres represent Tl, Ag, Br, Cs, N, and C atoms, respectively. H and disordered atoms are omitted for clarity. In (B) and (C), representations of hypothetical (110) and (111) 2D double perovskites, respectively, are shown. To date, there are no known examples of such materials, although these structure-types are known for single perovskites.

 © 2021 Wiley-VCH GmbH

perovskite sheets or also from a random distribution of the B-site cations within the same sheet.[62e,74]

2.4.2. The (110) and (111) Perovskites

Lower-dimensional perovskites with inorganic slabs derived from the (110) and (111) crystallographic planes of the 3D single perovskite structure are well-known.[69] However, to date, there are no examples of (110) double perovskites. Likewise, while the K_2PtCl_6-type perovskites belong to the (111) family (see Section 2.3, Figure 4D),[69] these materials do not qualify as dimensionally reduced double perovskites because we consider relatively undistorted vacancies to be distinct $[BX_6]^{6-}$ motifs that should be included when evaluating the structural connectivity. The perovskite $Cs_4Cu^{II}Sb^{III}{}_2Cl_{12}$, which consists of (111) layers of three chemically different ordered $[BX_6]^{n-}$ motifs ($[CuCl_6]^{4-}$, $[SbCl_6]^{3-}$, and $[\square Cl_6]^{6-}$)[70] also does not fit our definition of a dimensionally reduced double perovskite. The unreported (110) and (111) families of dimensionally reduced halide double perovskites (Figure 5B,C) present intriguing synthetic targets, which may exhibit properties quite different from their (001) counterparts, as shown for the lead-halide single perovskites.[75]

2.5. Structural Distortions

Structural distortions of the perovskite framework are well-known to have important consequences for a material's optical and electronic properties.[76] In the following sections, we discuss structural distortions found in halide double perovskites.

2.5.1. Structural Distortions of Elpasolites

Theoretically, double perovskites can undergo many different tilting distortions, as studied in detail by Woodward and co-workers.[77] However, nearly all elpasolites with X = Cl^-, Br^-, I^- belong to the cubic space group $Fm\bar{3}m$ at room temperature and, thus, exhibit perfect octahedral coordination of the B-site cations and no octahedral rotation. Notable exceptions include tetragonal $Cs_2Au^IAu^{III}X_6$ (X = Cl^-, Br^-, I^-)[23] and $Cs_2HgPdCl_6$[66] (in which the B and B′ centers adopt linear and square-planar geometries, respectively), rhombohedral $(MA)_2KBiCl_6$ (with room-temperature B-X-B′ bond angles differing from 180°),[78] and several halide cryolites (a subset of the elpasolites with the general formula $A^I{}_2A^IB^{III}X_6$) including $Na_2NaGdBr_6$.[79] Indeed, both octahedral distortions and tilting are observed in the halide cryolite family, which consists mostly of fluorides.[80]

2.5.2. Octahedral Rotations in K_2PtCl_6-Type Perovskites

The B-site vacancy in K_2PtCl_6-type perovskites decreases the rigidity of the 3D framework, enabling greater rotational freedom of the $[BX_6]^{2-}$ octahedra and a larger diversity of A-site cations. Undistorted octahedral coordination of the B^{4+} cation is maintained in lower-symmetry K_2PtCl_6-type perovskite structures, where either oversized[81] or undersized A-site cations (see list compiled by Brown[42]) induce octahedral tilting. We consider these non-cubic materials to be double perovskites only if the vacancy coordination resembles an octahedron (see Section 1.1). This definition is subjective; we expect that future experimental work will elucidate the maximum possible degree of distortion at the vacancies that still maintains the properties of a double perovskite. Besides these static distortions, anharmonic lattice dynamics, similar to those studied in single perovskites,[82] are widely reported in K_2PtCl_6-type perovskites[83] and are discussed elsewhere in more detail.[61b] As one example, the coupling of cesium displacements with octahedral rotations breaks the harmonic behavior of vibrations in both $CsSn^{II}I_3$[82a] and $Cs_2Sn^{IV}I_6$,[84] thus illustrating the generality of structural phenomena in single and double perovskites.

2.5.3. Distortions in 2D Double Perovskites

All 2D halide double perovskites reported to date exhibit significant local structural distortions,[34,62a–d,72] likely enabled by the enhanced structural flexibility afforded by the 2D framework relative to the 3D framework. The strict geometrical constraints imposed by the 3D perovskite structure are much less important in 2D structures, enabling the $[BX_6]^{n-}$ units to distort and tilt to achieve a more stable arrangement. Indeed, several reported 2D double perovskite compositions have not yet been realized in a 3D framework.[62b–d] For example, the instability of Cu^I-based 3D double perovskites, such as the hypothetical A_2CuInX_6, has been attributed to the preference of Cu^I for three- or fourfold coordination,[85] but several examples of Cu^I-based 2D double perovskites have recently emerged where the Cu^I centers adopt extremely distorted sixfold coordination spheres while still maintaining the perovskite structure (Figure 6C).[62d,72] The templating effect of the organic cations has also been implicated in directing the self-assembly of several distorted 2D double perovskite compositions,[62d,72] similar to templating effects well-known in 2D halide single perovskites.[69]

3. Electronic Structure

In the following sections, we discuss why double perovskites show a wider diversity of band structures than single perovskites, outline a simple and intuitive model for understanding and predicting their electronic structures, and highlight how symmetry-forbidden band gaps arise. An accessible introduction to band diagrams and reciprocal space by Hoffmann may prove useful to researchers unfamiliar with these topics.[86]

3.1. Implications of Broken B-Site Symmetry

In both single and double perovskites, the A-site cation typically does not directly contribute its orbitals to the valence band (VB) and conduction band (CB) electronic states.[9,87] In single perovskites, this leaves the $[BX_6]^{4-}$ unit as

 © 2021 Wiley-VCH GmbH

These are not the final page numbers!

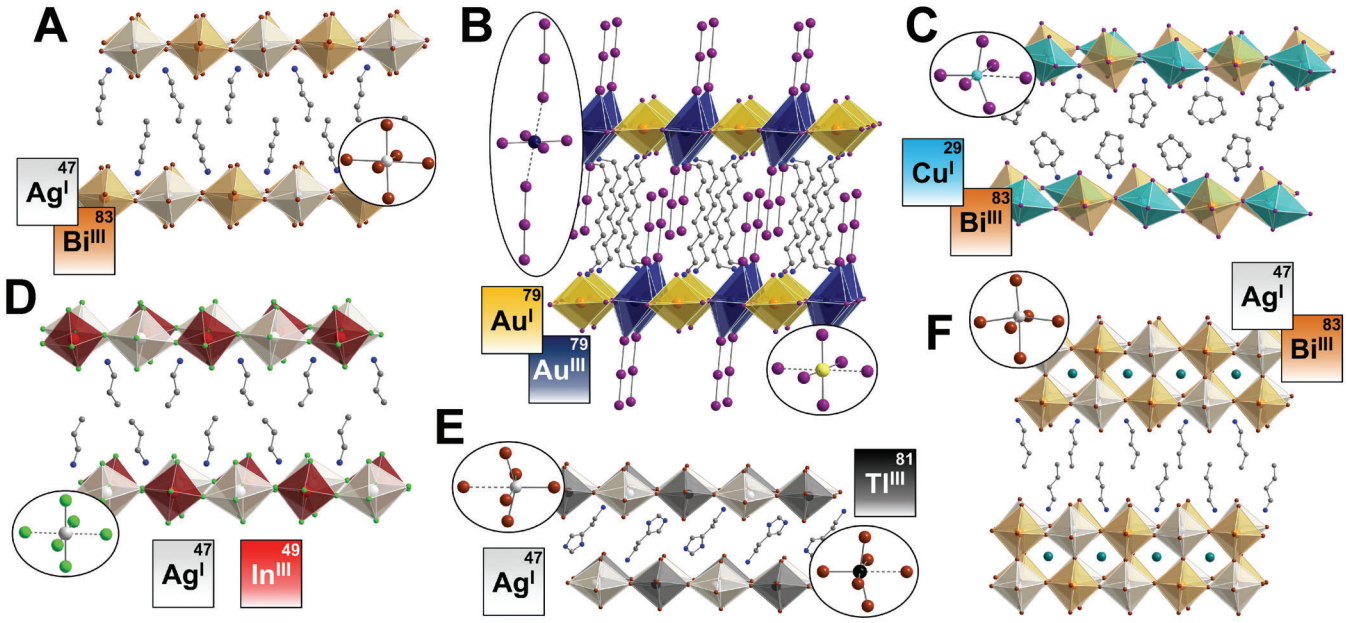

Figure 6. Structural diversity of 2D halide double perovskites with insets highlighting the structural distortions found in these materials. A) $(BA)_4AgBiBr_8$ (BA = butylammonium),[62a] B) $(ODA)_2[(Au^{I}I_2)(Au^{III}I_4)(I_3)_2]$ (ODA = 1,8-octanediammonium),[34] C) $(CHA)_4CuBiI_8$ (CHA = cycloheptylammonium),[72] D) $(PA)_4AgInCl_8$ (PA = propylammonium),[62c] E) $(HIS)_2AgTlBr_8$ (HIS = histammonium),[62b] F) $(BA)_2CsAgBiBr_7$.[62a] Atom colors: orange = Bi, white = Ag, yellow = Au^{I}, indigo = Au^{III}, red = In, turquoise = Cu, black = Tl, teal = Cs, purple = I, brown = Br, green = Cl, blue = N, and gray = C. H and disordered atoms are omitted for clarity.

the fundamental building block of the material's electronic states,[87] whereas the electronic structure in double perovskites is constructed from the combination of $[BX_6]^{n-}$ and $[B'X_6]^{m-}$ units.[9] This broken B-site symmetry leads to significantly more possible electronic structures for double perovskites compared to single perovskites.

In addition to creating a larger variety of electronic structures, the broken B-site symmetry can also fundamentally change the nature of the band-edge optical transition in double perovskites. In the well-studied lead-halide perovskites, the band gap can be viewed as a ligand-to-metal charge-transfer (LMCT) transition between halide p-orbital-dominated states in the VB (albeit with Pb s-orbital character) to Pb p-orbital-dominated states in the CB.[88] Similar LMCT band gaps occur in some double perovskites, particularly the K_2PtCl_6-type perovskites.[7b,9,61a,c,89] However, for many elpasolites, the band-edge transition has significant metal-to-metal charge-transfer (MMCT) character.[9] In the early literature, the jet black color and polarization-dependent absorption spectra of mixed-valence gold double perovskites were attributed to a $Au^{I} \rightarrow Au^{III}$ intervalence charge transfer (IVCT).[28c] More recently, our work on the double perovskites Cs_2AgTlX_6 (X = Cl^-, Br^-) showed that the VB states have a large degree of Ag^+d character and the CB states have significant Tl^{3+}s character. As a consequence of the relatively small difference in energy between the $[AgX_6]^{5-}$ HOMO and $[TlX_6]^{3-}$ LUMO, the MMCT nature of the band gap results in an abnormally small band gap of 0.95 eV for X = Br^- (2.0 eV for X = Cl^-).[54] Tuning this MMCT transition in elpasolites through proper selection of B/B′ combinations offers a powerful way to control the band gap.[54]

3.2. Predictions of the Electronic Structure from Orbital Symmetry

Seeking a chemically intuitive interpretation of double perovskite band structures, our group developed a qualitative linear combination of atomic orbitals (LCAO) framework.[9] Using this approach, a qualitatively accurate band structure of nearly every known halide double perovskite can be determined by considering only the bonding and antibonding interactions between nearest neighbors (B-X interactions) and next-nearest neighbors (interactions between halides at right angles from one another within the same octahedron). The positions of the valence band maximum (VBM) and conduction band minimum (CBM) depend strongly on the match or mismatch in symmetry between the B and B′ frontier atomic orbitals. Isoelectronic combinations of B and B′ cations give rise to direct band gaps, whereas other B and B′ combinations can produce either indirect or direct band gaps. Overall, this LCAO model allows prediction of the VBM and CBM of a double perovskite, often from its chemical formula alone (Table 1).

3.3. Symmetry-Forbidden Band Gaps

Analogous to molecular transitions, the absorption of light by centrosymmetric solids obeys the Laporte selection rule.[90] Thus, optical transitions between states with identical inversion symmetry (e.g. E_g and A_{1g}) are symmetry-forbidden (also called Laporte- or parity-forbidden), leading to weak optical absorption (Figure 7 A).[90] Yan and co-workers have

 © 2021 Wiley-VCH GmbH

Table 1: Expected *k*-point locations of the conduction band minimum (CBM) and valence band maximum (VBM) for all possible combinations of B and B′ orbitals.[a] Only σ-bonding states are shown, see Ref. [9] for analysis of the π-bonding states.

Orbitals		Prediction	
B	B′	VBM	CBM
s	*s*	Γ	Γ
p	*p*	Γ	Γ
$d_{x^2-y^2}/d_{z^2}$	$d_{x^2-y^2}/d_{z^2}$	Γ & X	Γ & X
s	*p*	L	L
s	$d_{x^2-y^2}/d_{z^2}$	X	X
p	$d_{x^2-y^2}/d_{z^2}$	–	–
s	null	X	Γ
p	null	L	L
$d_{x^2-y^2}/d_{z^2}$	null	Γ & X	X
null	null	Γ & X	–

[a] To use this table, first determine the highest occupied molecular orbitals (HOMOs) of the B and B′ cations of interest. Next, locate the line in the table that matches these two HOMOs and read across to find the VBM. Repeating the process with the lowest unoccupied molecular orbitals (LUMOs) of the B and B′ cations will give the CBM. Note that the VBM and CBM must be evaluated separately for a given perovskite. The term "null" refers to the case in which the B/B′-site occupant lacks an orbital with the appropriate energy to participate in the band. Reproduced from Ref. [9] with permission from the Royal Society of Chemistry.

illustrated that forbidden optical transitions have significant implications for elpasolite-based optoelectronics.[91] Taking $Cs_2AgTlCl_6$ as an example, the band-gap transition at Γ involves an E_g orbital in the VB and an A_{1g} orbital in the CB (Figure 7B).[9] Both have *gerade* symmetry, thus giving rise to a symmetry-forbidden band gap. On moving from Γ to L, optical transitions gradually become allowed (Figure 7C), evident in calculations of dipole matrix elements,[54] because translational symmetry introduces *ungerade* symmetry to the electronic states.[9] This is also observed in isoelectronic $Cs_2AgInCl_6$, where the transition at L has been assigned as E_g to A_{2u}.[91]

Symmetry-forbidden band gaps are also reported in K_2PtCl_6-type perovskites[18,61a] and may explain the disagreement in band-gap values of Cs_2SnI_6 measured by diffuse reflectance (DR; 1.3 eV)[7b,18] and thin-film absorption (1.6 eV).[92] Relative to thin-film measurements, DR is quite sensitive to weak absorption (low absorption coefficients) because of the larger particle size of powder samples.[62a] Thus, DR may show the onset of the symmetry-forbidden band gap of Cs_2SnI_6, whereas thin-film absorption detects only the higher-energy, allowed transitions. The 0.35 eV width of the forbidden region calculated by DFT[18] agrees well with the approximately 0.3 eV discrepancy between DR and thin-film measurements.

Importantly, symmetry-forbidden band gaps can be advantageous for solar absorbers if allowed transitions exist close to the band edge. For example, calculations place the width of the forbidden region in $Cs_2AgTlCl_6$ and $Cs_2AgInCl_6$ at 0.17 and 0.27 eV, respectively.[54] A narrow forbidden region does not substantially affect light absorption, but it can slow recombination as carriers funnel to the forbidden region, thus affording long carrier lifetimes beneficial for charge extraction, as seen in Cs_2AgTlX_6 ($X = Cl^-$, Br^-).[54,93] Thus, this feature of double perovskite electronic structures may prove useful in future efforts to tune these materials for optoelectronic applications.

4. Manipulating the Electronic Structure

Recent work has demonstrated the exquisite sensitivity of double perovskite electronic structures to variations in the composition and dimensionality of the structure. Here we discuss these two strategies for modulating the electronic structures of double perovskites.

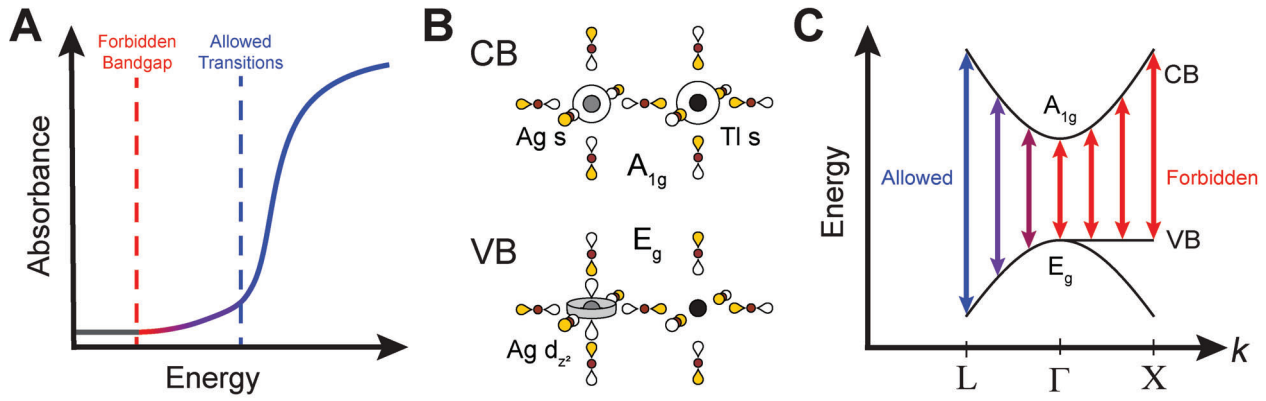

Figure 7. Schematic illustration of symmetry-forbidden band gaps using $Cs_2AgTlCl_6$ as an example. A) The weak absorption onset expected for a material with a symmetry-forbidden band gap. B) Schematic orbital representation of the valence band (VB) and conduction band (CB) at Γ in $Cs_2AgTlCl_6$. The VB contains Cl p and Ag d orbitals, whereas the CB contains Cl p, Ag s, and Tl s orbitals. C) Band diagram depicting allowed and forbidden optical transitions in $Cs_2AgTlCl_6$. At Γ, the band-gap transition is forbidden because of the shared *gerade* symmetry of the VB and CB. Transitions become allowed on moving from Γ to L because *ungerade* character is introduced.

© 2021 Wiley-VCH GmbH

These are not the final page numbers!

4.1. Alloying

Double perovskites are very tolerant hosts for impurity alloying, and the effects of substoichiometric substitution of a range of different B-site cations have been explored.[7a,18,27a,55,57,94] In isovalent alloys, in which the impurity cation replaces a cation of the same charge, stable solid solutions generally form across most or all of the composition range. In aliovalent alloys, introducing dopants often generates cation vacancies (such as Ag^+ vacancies[57c]) because of the charge mismatch between the impurity cation and the cation it replaces. This limits the range of achievable compositions to low dopant concentrations (typically <1 atom%).[57c,94a] However, substitution of Sn^{4+} cations in Cs_2SnCl_6 by equal amounts of Sb^{3+} and Sb^{5+} demonstrates that, in some cases, formation of charge-compensating vacancies can be avoided in aliovalent alloys, thus affording greater compositional flexibility.[47] Nevertheless, even at impurity concentrations as low as 1 atom%, both iso- and aliovalent alloying can dramatically modify the size and symmetry of the host material's band gap.[57b,c]

Isoelectronic alloys involve substitution of a cation in the host structure by an impurity cation that has the same electronic configuration. Thus, a change in the symmetry of the band gap is not expected (see Section 3.2), only a modification of its size. For example, in $Cs_2Ag(Bi_{1-x}Sb_x)Br_6$ the band gap drops gradually with increasing Sb^{3+} substitution, but remains indirect throughout.[57a] This decrease in the band gap is almost entirely caused by an increase in the energy of the s-orbital-based VBM and can be understood by noting that the Sb^{3+} 5s orbital is higher in energy than the Bi^{3+} 6s orbital due to relativistic effects.

In non-isoelectronic alloys, the impurity does not have the same electronic configuration as the cation it replaces, so both the symmetry and size of the band gap should change at sufficiently high levels of alloying. In the two closely related alloys $Cs_2Ag(Bi_{1-x}In_x)Br_6$[57a] and $Cs_2Ag(Bi_{1-x}Tl_x)Br_6$,[54,57b] an $(n-1)d^{10}ns^0$ cation (In^{3+} or Tl^{3+}) replaces an ns^2np^0 cation (Bi^{3+}). As shown in Figure 8, with increasing Tl^{3+} content, the empty s orbitals begin to form a new CB in $Cs_2Ag(Bi_{1-x}Tl_x)Br_6$. Since this band involves Ag^+ s and Tl^{3+} s orbitals, it has a minimum at Γ (Table 1).[9] Meanwhile, the removal of Bi^{3+} from the structure reduces the antibonding contribution of Bi^{3+} 6s orbitals to the VB at X, thereby lowering the VBM. Over most of the solid-solution range, the band gap is indirect from X to Γ, but once enough Bi^{3+} is removed from the system, the band gap becomes direct at Γ, as in $Cs_2AgTlBr_6$ and $Cs_2AgInCl_6$.[53a,54]

As for isoelectronic alloys, the change in the band gap size observed in non-isoelectronic alloys is largely dictated by the energy of the frontier orbitals of the impurity cation with respect to those of the host. Upon incorporation of Tl^{3+}, $Cs_2Ag(Bi_{1-x}Tl_x)Br_6$ shows a rapid decrease in the band gap because the Tl^{3+} 6s orbitals sit within the $Cs_2AgBiBr_6$ band gap (Figure 8). In contrast, $Cs_2Ag(Bi_{1-x}In_x)Br_6$ shows a small increase in the band gap with increasing In^{3+} content.[57a] Here, the In^{3+} 5s orbitals are nearly degenerate with the CB of $Cs_2AgBiBr_6$, and the increase in the band gap is driven by removal of Bi^{3+} antibonding character from the VBM.

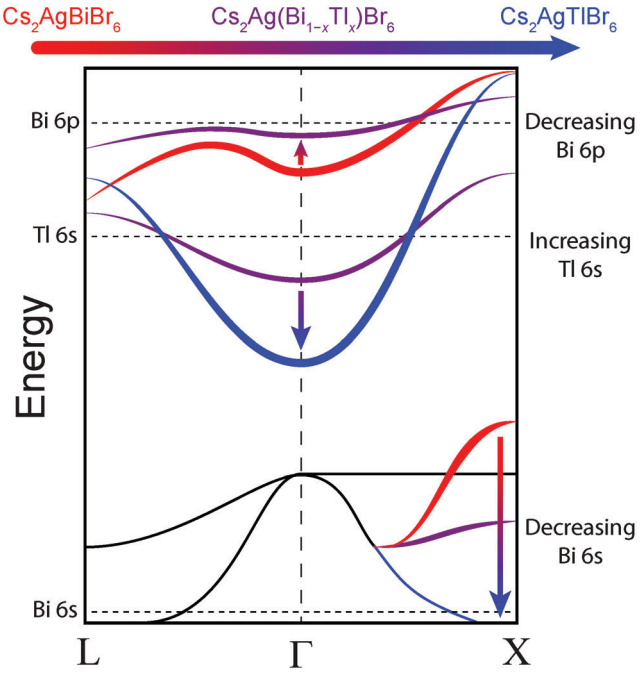

Figure 8. Schematic band diagram showing the change in electronic structure over the composition range of the $Cs_2Ag(Bi_{1-x}Tl_x)Br_6$ solid solution. Only the bands or portions of bands that change on alloying are colored. The red and blue lines correspond to the bands of $Cs_2AgBiBr_6$ and $Cs_2AgTlBr_6$, respectively, while purple shows an intermediate composition. Horizontal dashed black lines show the approximate energies of the isolated molecular orbitals.

4.2. Dimensional Reduction

Dimensional reduction is a powerful handle for tuning electronic structures;[95] however, the electronic effects of the dimensional reduction of halide double perovskites have only recently been explored.[62a,b] In the first study on this topic, we reported that the indirect band gap of 3D $Cs_2AgBiBr_6$ is maintained in all materials with $\infty \geq n \geq 2$ but becomes direct in the $n=1$ perovskite. Calculations on the band structure of undistorted model systems indicated that dimensional reduction drives this band-gap transition, although local structural distortions of the perovskite framework modulate band dispersion.[62a] Since this work, several additional studies of 2D double perovskite electronic structures have emerged.[62b–e] In particular, our work on the electronically distinct Ag-Tl family of halide double perovskites demonstrates that dimensional reduction drives an analogous direct-to-indirect band-gap transition at the $n=1$ limit of $Cs_2AgTlBr_6$.[62b] This substantial change in the electronic structure observed at the $n=1$ limit in two electronically distinct double perovskite families is intriguing, and understanding the generality of this transition across the wide array of possible compositions is a worthy topic for future research.

© 2021 Wiley-VCH GmbH

5. Outlook

Modern research on halide double perovskites brings together two materials families, elpasolites and K_2PtCl_6-type perovskites, which were historically independent. The unification of these two structure-types was enabled by observations of their structural,[16,96] optical,[18,54,91] and electronic[9,54,61b] similarities and helped advance understanding of both families, as insight gained into one could inform research on the other. As we move forward, seeking to further understand, develop, and utilize halide double perovskites, we should learn from this historical precedent and continue to search for parallels between halide double perovskites and other well-studied materials families (Figure 9). Thus, to close this Minireview, we highlight similarities between halide double perovskites and other important classes of materials. We end with a very brief discussion of potential applications of halide double perovskites.

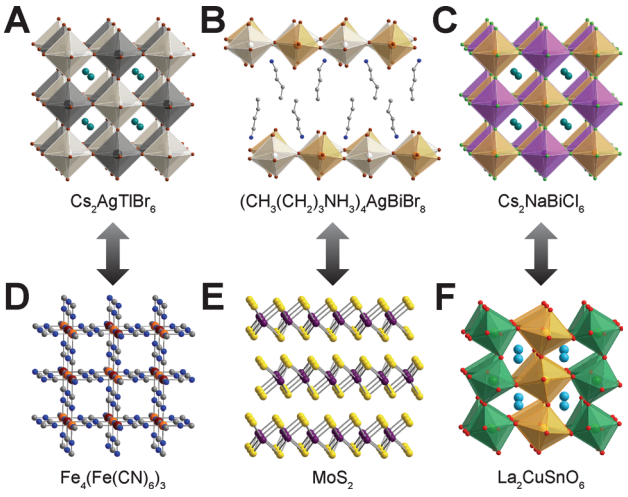

Figure 9. Comparison of halide perovskites (A,[54] B,[62a] and C[106]) with the well-known Prussian Blue (D), transition-metal dichalcogenide (E), and oxide perovskite (F) families, which provide historical precedent. Atom colors: teal = Cs, white = Ag, black = Tl, light orange = Bi, light purple = Na, dark purple = Mo, light blue = La, gold = Cu, dark green = Sn, crimson = Fe^{II}, orange = Fe^{III}, brown = Br, green = Cl, blue = N, red = O, yellow = S, and gray = C. H and disordered atoms are omitted for clarity.

5.1. The Prussian Blue Analogues (PBAs)

The MMCT nature of the band-gap transition of many elpasolites affords a direct means of manipulating the gap by selecting $[BX_6]^{n-}$ and $[B'X_6]^{m-}$ molecular hexahalides with the desired HOMO and LUMO energy levels (see Section 3.1). However, the exploitation of MMCT transitions in the perovskite field[54] is long predated by studies of such transitions in the PBAs, a closely related materials family. Prussian Blue (PB; $Fe_4^{III}[Fe^{II}(CN)_6]_3{\cdot}14H_2O$) can be considered a double perovskite in which cyanides (pseudohalides) replace the halides, all A-sites are vacant, and 25% of the $[Fe^{II}(CN)_6]^{4-}$ units are missing. PB has a rich history as one of the earliest synthetic blue pigments and its intense color arises from an $Fe^{II} \rightarrow Fe^{III}$ MMCT. It was first made by accident by the German pigment maker Heinrich Diesbach while attempting to make a violet pigment from a mixture containing $Fe^{III}_2(SO_4)_3$ and potash. However, unbeknownst to him, his potash had previously been used by the alchemist Johann Dippel to prepare a concoction involving animal blood. As a result, it was contaminated with Fe^{II} and cyanide, thus providing the necessary ingredients to make PB.[97] Since its synthesis, PB has been used in historical works of art such as the "Great Wave off Kanagawa" (ca. 1830). Revisiting the vast literature on tuning the MMCT transition of PBAs[28c,98] may teach us how to adapt halide double perovskites to absorb sunlight in solar cells. Similar to the careful studies on $[M(CN)_6]^{n-}$ molecules,[99] studying the energy levels of $[BX_6]^{n-}$ molecules that form the building blocks of elpasolites should allow us to predict and manipulate the magnitude of their band gaps.

A similar analogy exists between layered double perovskites and Hofmann clathrates such as $Ni^{II}(CN)_4{\cdot}Ni^{II}(NH_3)_2$, the layered counterparts of PBAs.[100] However, in contrast to the organoammonium cations in layered halide perovskites, neutral amines that coordinate to the metal cations comprise the organic layers in Hofmann clathrates.

5.2. The Transition-Metal Dichalcogenides (TMDCs)

Recent work has uncovered dramatic changes in band-gap symmetry (direct/indirect) upon dimensional reduction of the 3D halide double perovskite structure to the 2D monolayer structure (see Section 4.2).[62a,b] These findings are reminiscent of the well-known indirect-to-direct band gap transition in TMDCs, such as MoS_2, which occurs when the bulk material is exfoliated to a single monolayer.[101] The thorough understanding of this band-gap transition in the TMDCs laid the groundwork for unique applications of these materials.[102] Thus, as researchers continue to expand the field of halide double perovskites, we should seek a similar understanding of the orbital basis for changes in band-gap symmetry with dimensionality.

5.3. Molecular BX_6 Complexes

The electronic properties of K_2PtCl_6-type perovskites are largely determined by the $[BX_6]^{2-}$ complex, thereby offering a platform to study the behavior of metal-halide octahedra in the solid state, in parallel with many prior studies on molecules in solution. For example, the splitting of the band corresponding to the s→p transition in $[TeX_6]^{2-}$ (X = Cl^-, Br^-) molecules evidenced lower symmetry ($O_h \rightarrow C_{2v}$) in their photoexcited states.[103] Similar distorted excited states have been invoked to explain the Stokes-shifted photoluminescence of halide perovskites.[63b] In addition, similar to the LMCT nature of the band gap in K_2PtCl_6-type perovskites, the primary photoreduction pathway for $PtCl_6^{2-}$ molecules is also an inner-sphere LMCT.[104] The solid-state packing interactions in double perovskites also stabilize different geometries. For example, the intriguing high-pressure redox

 © 2021 Wiley-VCH GmbH
These are not the final page numbers!

transformation of $Cs_2Pd^{II}I_4{\cdot}I_2$ to $Cs_2Pd^{IV}I_6$ demonstrates interchangeable coordination from square-planar $[Pd^{II}I_4]^{2-}$ to octahedral $[Pd^{IV}I_6]^{2-}$.[105] Although interoctahedral interactions in K_2PtCl_6-type perovskites are historically disregarded,[103] recent work illustrates that interactions across the vacancies, particularly in iodide perovskites, generate disperse CBs.[18] Moving forward, it is worth developing a more nuanced understanding of interoctahedral interactions in K_2PtCl_6-type perovskites, which exist on the conceptual border between molecular salts with localized orbitals and semiconductors with delocalized bands.

5.4. Other Perovskites

While seemingly trivial, we must not lose sight of the fact that both oxide double perovskites and halide single perovskites boast structure types not yet observed in halide double perovskites. As illustrated by $Cs_2NaBiCl_6$ (Figure 9C),[106] halide double perovskites exhibit rock salt B-site ordering. Oxide double perovskites display B-site orderings unknown in the halides (see Section 2.2),[8a,b,67] and diverse structural topologies exist for lower-dimensional halide single perovskites that remain unknown in the double perovskites (see Section 2.4).[63a] Such materials represent worthy synthetic targets that may afford novel properties.

5.5. Applications

Although this Minireview is focused on fundamental studies, we note that 3D double perovskites have previously been considered for applications in lasing,[27a,b] scintillation,[27c] and upconversion.[27d,48] More recently, 3D double perovskites have been considered as components of electroluminescent devices,[7a] X-ray detectors,[7d,107] and solar cells as either absorbers[7c] or hole-transport layers.[7b] The performance of double perovskites in some of these newer applications is still evolving because efficiencies depend heavily on film morphology and defects, which will likely be better understood and controlled through future studies. For example, as a consequence of its indirect band gap, $Cs_2AgBiBr_6$ films used as solar absorbers must be micrometers thick to adequately absorb sunlight[52a] (similar to Si absorbers), and preparing thick, high-quality films of these quaternary compounds remains a challenge. Recent studies also show that long carrier diffusion lengths (ca. 11 μm) may be realized in $Cs_2AgBiBr_6$ if surface trap states are passivated,[93] thus motivating studies on the defect chemistry of double perovskites.

The stunning diversity of chemical compositions and electronic structures afforded by the two distinct B sites of double perovskites brings with it a mighty challenge: can we predict which B-site combinations will provide the desired properties? Despite their long history, foundational studies on halide double perovskites are still needed for us to shrewdly place our bets and win, as the stakes are doubled.

Acknowledgements

This work was supported by the Department of Energy, Office of Basic Energy Sciences, Division of Materials Sciences and Engineering, under contract DE-AC02-76SF00515. N.R.W. is supported by a Stanford Interdisciplinary Graduate Fellowship. B.A.C. was supported by an NSF graduate fellowship (DGE-114747) and the Evelyn McBain award from Stanford Chemistry. A.H.S. was supported by a Stanford Graduate Fellowship and the Veatch award from Stanford Chemistry.

Conflict of interest

The authors declare no conflict of interest.

[1] a) W. Cross, W. F. Hillebrand, *Am. J. Sci.* **1883**, *s3-26*, 271; b) H. L. Wells, *Am. J. Sci.* **1893**, *s3-45*, 121.
[2] a) D. Weber, *Z. Naturforsch. B* **1978**, *33*, 1443; b) A. Kojima, K. Teshima, Y. Shirai, T. Miyasaka, *J. Am. Chem. Soc.* **2009**, *131*, 6050.
[3] a) D. P. McMeekin, G. Sadoughi, W. Rehman, G. E. Eperon, M. Saliba, M. T. Hörantner, A. Haghighirad, N. Sakai, L. Korte, B. Rech, M. B. Johnston, L. M. Herz, H. J. Snaith, *Science* **2016**, *351*, 151; b) M. Saliba, T. Matsui, J.-Y. Seo, K. Domanski, J.-P. Correa-Baena, M. K. Nazeeruddin, S. M. Zakeeruddin, W. Tress, A. Abate, A. Hagfeldt, M. Grätzel, *Energy Environ. Sci.* **2016**, *9*, 1989; c) J. Xu, C. C. Boyd, Z. J. Yu, A. F. Palmstrom, D. J. Witter, B. W. Larson, R. M. France, J. Werner, S. P. Harvey, E. J. Wolf, W. Weigand, S. Manzoor, M. F. A. M. van Hest, J. J. Berry, J. M. Luther, Z. C. Holman, M. D. McGehee, *Science* **2020**, *367*, 1097.
[4] a) A. H. Slavney, R. W. Smaha, I. C. Smith, A. Jaffe, D. Umeyama, H. I. Karunadasa, *Inorg. Chem.* **2017**, *56*, 46; b) A. D. Jodlowski, D. Rodríguez-Padrón, R. Luque, G. de Miguel, *Adv. Energy Mater.* **2018**, *8*, 1703120.
[5] a) F. Igbari, Z.-K. Wang, L.-S. Liao, *Adv. Energy Mater.* **2019**, *9*, 1803150; b) F. Giustino, H. J. Snaith, *ACS Energy Lett.* **2016**, *1*, 1233.
[6] a) S. E. Creutz, E. N. Crites, M. C. De Siena, D. R. Gamelin, *Nano Lett.* **2018**, *18*, 1118; b) F. Locardi, M. Cirignano, D. Baranov, Z. Dang, M. Prato, F. Drago, M. Ferretti, V. Pinchetti, M. Fanciulli, S. Brovelli, L. De Trizio, L. Manna, *J. Am. Chem. Soc.* **2018**, *140*, 12989; c) B. Yang, X. Mao, F. Hong, W. Meng, Y. Tang, X. Xia, S. Yang, W. Deng, K. Han, *J. Am. Chem. Soc.* **2018**, *140*, 17001.
[7] a) J. Luo, X. Wang, S. Li, J. Liu, Y. Guo, G. Niu, L. Yao, Y. Fu, L. Gao, Q. Dong, C. Zhao, M. Leng, F. Ma, W. Liang, L. Wang, S. Jin, J. Han, L. Zhang, J. Etheridge, J. Wang, Y. Yan, E. H. Sargent, J. Tang, *Nature* **2018**, *563*, 541; b) B. Lee, C. C. Stoumpos, N. Zhou, F. Hao, C. Malliakas, C.-Y. Yeh, T. J. Marks, M. G. Kanatzidis, R. P. H. Chang, *J. Am. Chem. Soc.* **2014**, *136*, 15379; c) E. Greul, M. L. Petrus, A. Binek, P. Docampo, T. Bein, *J. Mater. Chem. A* **2017**, *5*, 19972; d) W. Pan, H. Wu, J. Luo, Z. Deng, C. Ge, C. Chen, X. Jiang, W.-J. Yin, G. Niu, L. Zhu, L. Yin, Y. Zhou, Q. Xie, X. Ke, M. Sui, J. Tang, *Nat. Photonics* **2017**, *11*, 726.
[8] a) M. T. Anderson, K. B. Greenwood, G. A. Taylor, K. R. Poeppelmeier, *Prog. Solid State Chem.* **1993**, *22*, 197; b) S. Vasala, M. Karppinen, *Prog. Solid State Chem.* **2015**, *43*, 1; c) N. Mercier, *Angew. Chem. Int. Ed.* **2019**, *58*, 17912; *Angew. Chem.* **2019**, *131*, 18078; d) B. Vargas, G. Rodríguez-López, D. Solis-Ibarra, *ACS Energy Lett.* **2020**, *5*, 3591.

 © 2021 Wiley-VCH GmbH

[9] A. H. Slavney, B. A. Connor, L. Leppert, H. I. Karunadasa, *Chem. Sci.* **2019**, *10*, 11041.

[10] a) J. D. Donaldson, D. Laughlin, S. D. Ross, J. Silver, *J. Chem. Soc. Dalton Trans.* **1973**, 1985; b) J. Barrett, J. D. Donaldson, J. Silver, N. P. Y. Siew, *J. Chem. Soc. Dalton Trans.* **1977**, 906.

[11] a) C. C. Stoumpos, C. D. Malliakas, M. G. Kanatzidis, *Inorg. Chem.* **2013**, *52*, 9019; b) G. E. Eperon, T. Leijtens, K. A. Bush, R. Prasanna, T. Green, J. T.-W. Wang, D. P. McMeekin, G. Volonakis, R. L. Milot, R. May, A. Palmstrom, D. J. Slotcavage, R. A. Belisle, J. B. Patel, E. S. Parrott, R. J. Sutton, W. Ma, F. Moghadam, B. Conings, A. Babayigit, H.-G. Boyen, S. Bent, F. Giustino, L. M. Herz, M. B. Johnston, M. D. McGehee, H. J. Snaith, *Science* **2016**, *354*, 861; c) C. Wang, Z. Song, C. Li, D. Zhao, Y. Yan, *Adv. Funct. Mater.* **2019**, *29*, 1808801.

[12] a) G. Gou, N. Charles, J. Shi, J. M. Rondinelli, *Inorg. Chem.* **2017**, *56*, 11854; b) A. Aimi, D. Mori, K.-i. Hiraki, T. Takahashi, Y. J. Shan, Y. Shirako, J. Zhou, Y. Inaguma, *Chem. Mater.* **2014**, *26*, 2601.

[13] M. Ducau, K. S. Suh, J. Senegas, J. Darriet, *Mater. Res. Bull.* **1992**, *27*, 1115.

[14] W. Cross, W. F. Hillebrand, *U.S. Geol. Surv. Bull.* **1885**, *20*, 1.

[15] H. L. Wheeler, *Am. J. Sci.* **1893**, *s3-45*, 267.

[16] M. Krupski, *Phys. Status Solidi A* **1989**, *116*, 657.

[17] D. H. Brown, K. R. Dixon, C. M. Livingston, R. H. Nuttall, D. W. A. Sharp, *J. Chem. Soc. A* **1967**, 100.

[18] A. E. Maughan, A. M. Ganose, M. M. Bordelon, E. M. Miller, D. O. Scanlon, J. R. Neilson, *J. Am. Chem. Soc.* **2016**, *138*, 8453.

[19] P. Scherrer, P. Stoll, *Z. Anorg. Allg. Chem.* **1922**, *121*, 319.

[20] H. L. Wells, *Am. J. Sci.* **1922**, *s5-3*, 315.

[21] G. Menzer, *Fortschr. Mineral. Kristallogr. Petrogr.* **1932**, *17*, 61.

[22] L. R. Morss, *J. Inorg. Nucl. Chem.* **1974**, *36*, 3876.

[23] N. Elliott, L. Pauling, *J. Am. Chem. Soc.* **1938**, *60*, 1846.

[24] a) K. Knox, D. W. Mitchell, *J. Inorg. Nucl. Chem.* **1961**, *21*, 253; b) J.-P. Besse, M. Capestan, *C. R. Seances Acad. Sci. Ser. C* **1968**, *266*, 551; c) L. R. Morss, M. Siegal, L. Stenger, N. Edelstein, *Inorg. Chem.* **1970**, *9*, 1771.

[25] G. Meyer, *Prog. Solid State Chem.* **1982**, *14*, 141.

[26] a) E. Bucher, H. J. Guggenheim, K. Andres, G. W. Hull, Jr., A. S. Cooper, *Phys. Rev. B* **1974**, *10*, 2945; b) H.-D. Amberger, G. G. Rosenbauer, R. D. Fischer, *J. Phys. Chem. Solids* **1977**, *38*, 379.

[27] a) B. F. Aull, H. P. Jenssen, *Phys. Rev. B* **1986**, *34*, 6647; b) C. Reber, H. U. Güdel, G. Meyer, T. Schleid, C. A. Daul, *Inorg. Chem.* **1989**, *28*, 3249; c) C. M. Combes, P. Dorenbos, C. W. E. van Eijk, K. W. Krämer, H. U. Güdel, *J. Lumin.* **1999**, *82*, 299; d) D. R. Gamelin, H. U. Güdel, *J. Am. Chem. Soc.* **1998**, *120*, 12143.

[28] a) S. Yamada, R. Tsuchida, *Bull. Chem. Soc. Jpn.* **1956**, *29*, 421; b) G. Brauer, G. Sleater, *J. Less-Common Met.* **1970**, *21*, 283; c) M. B. Robin, P. Day in *Advances in Inorganic Chemistry and Radiochemistry*, *Vol. 10* (Eds.: H. J. Emeléus, A. G. Sharpe), Academic Press, New York, **1968**, p. 247.

[29] a) R. Keller, J. Fenner, W. B. Holzapfel, *Mater. Res. Bull.* **1974**, *9*, 1363; b) W. Denner, H. Schulz, H. D′Amour, *Acta Crystallogr. Sect. A* **1979**, *35*, 360; c) J. Stanek, S. S. Hafner, H. Schulz, *Phys. Lett. A* **1980**, *76*, 333; d) J. Stanek, *J. Chem. Phys.* **1982**, *76*, 2315.

[30] R. J. Cava, B. Batlogg, J. J. Krajewski, R. Farrow, L. W. Rupp, Jr., A. E. White, K. Short, W. F. Peck, T. Kometani, *Nature* **1988**, *332*, 814.

[31] N. Kojima, H. Kitagawa, T. Ban, F. Amita, M. Nakahara, *Solid State Commun.* **1990**, *73*, 743.

[32] a) S. S. Hafner, N. Kojima, J. Stanek, L. Zhang, *Phys. Lett. A* **1994**, *192*, 385; b) N. Kojima, M. Hasegawa, H. Kitagawa, T. Kikegawa, O. Shimomura, *J. Am. Chem. Soc.* **1994**, *116*, 11368.

[33] a) M. Retuerto, T. Emge, J. Hadermann, P. W. Stephens, M. R. Li, Z. P. Yin, M. Croft, A. Ignatov, S. J. Zhang, Z. Yuan, C. Jin, J. W. Simonson, M. C. Aronson, A. Pan, D. N. Basov, G. Kotliar, M. Greenblatt, *Chem. Mater.* **2013**, *25*, 4071; b) M. Retuerto, Z. Yin, T. J. Emge, P. W. Stephens, M.-R. Li, T. Sarkar, M. C. Croft, A. Ignatov, Z. Yuan, S. J. Zhang, C. Jin, R. P. Sena, J. Hadermann, G. Kotliar, M. Greenblatt, *Inorg. Chem.* **2015**, *54*, 1066.

[34] L. M. Castro-Castro, A. M. Guloy, *Angew. Chem. Int. Ed.* **2003**, *42*, 2771; *Angew. Chem.* **2003**, *115*, 2877.

[35] N. Matsushita, H. Kitagawa, N. Kojima, *Acta Crystallogr. Sect. C* **1997**, *53*, 663.

[36] J. J. Berzelius, *Ann. Phys. Chem.* **1834**, *108*, 577.

[37] a) M. Jacquelain, *Ann. Chim. Phys.* **1837**, 113; b) T. Hiortdahl, *Z. Kristallogr. Cryst. Mater.* **1882**, *6*, 456; c) A. Gutbier, A. Krell, *Ber. Dtsch. Chem. Ges.* **1905**, *38*, 2385; d) P. Groth, *Chemische Krystallographie*, *Vol. 1*, Wilhelm Engelmann, Leipzig, **1906**, pp. 466–535; e) R. L. Datta, *J. Am. Chem. Soc.* **1913**, *35*, 1185; f) M. Delèpine, *Ann. Chim.* **1917**, *7*, 277.

[38] a) R. L. Slagle, PhD thesis, Johns Hopkins University (Baltimore, Maryland, USA), **1894**; b) A. Rosenheim, H. Aron, *Z. Anorg. Allg. Chem.* **1904**, *39*, 170.

[39] a) R. W. G. Wyckoff, E. Posnjak, *J. Am. Chem. Soc.* **1921**, *43*, 2292; b) R. G. Dickinson, *J. Am. Chem. Soc.* **1922**, *44*, 276; c) F. J. Ewing, L. Pauling, *Z. Kristallogr. Cryst. Mater.* **1928**, *68*, 223; d) P. Stoll, PhD thesis, ETH Zürich (Zürich, Switzerland), **1926**; e) W. A. Frederikse, H. J. Verweel, *Recl. Trav. Chim. Pays-Bas* **1928**, *47*, 904.

[40] a) G. Engel, *Z. Kristallogr. Cryst. Mater.* **1935**, *90*, 341; b) J. A. A. Ketelaar, A. A. Rietdijk, C. H. van Staveren, *Recl. Trav. Chim. Pays-Bas* **1937**, *56*, 907; c) J. A. A. Ketelaar, J. F. van Walsem, *Recl. Trav. Chim. Pays-Bas* **1938**, *57*, 964; d) W. Werker, *Recl. Trav. Chim. Pays-Bas* **1939**, *58*, 257; e) R. W. G. Wyckoff, *The Structure of Crystals*, 2nd ed., The Chemical Catalog Company, Inc., New York, **1931**, pp. 303–306; f) R. W. G. Wyckoff, *The Structure of Crystals. Supplement for 1930–1934 to the Second Edition*, Reinhold Publishing Corporation, New York, **1935**, pp. 77–80.

[41] a) M. G. Brik, I. V. Kityk, *J. Phys. Chem. Solids* **2011**, *72*, 1256; b) B. E. Douglas, S.-M. Ho in *Structure and Chemistry of Crystalline Solids*, Springer, New York, **2006**, pp. 128–129.

[42] I. D. Brown, *Can. J. Chem.* **1964**, *42*, 2758.

[43] V. M. Goldschmidt, *Naturwissenschaften* **1926**, *14*, 477.

[44] M. Krupski, *Phys. Status Solidi A* **1983**, *78*, 751.

[45] a) D. Nakamura, Y. Kurita, K. Ito, M. Kubo, *J. Am. Chem. Soc.* **1960**, *82*, 5783; b) K. Ito, D. Nakamura, K. Ito, M. Kubo, *Inorg. Chem.* **1963**, *2*, 690; c) M. Kubo, D. Nakamura in *Advances in Inorganic Chemistry and Radiochemistry*, *Vol. 8* (Eds.: H. J. Emeléus, A. G. Sharpe), Academic Press, New York, **1966**, pp. 257–282.

[46] a) J. Owen, K. W. H. Stevens, *Nature* **1953**, *171*, 836; b) J. H. E. Griffiths, J. Owen, *Proc. R. Soc. London Ser. A* **1954**, *226*, 96.

[47] L. Atkinson, P. Day, *J. Chem. Soc. A* **1969**, 2423.

[48] D. R. Gamelin, H. U. Güdel, *Inorg. Chem.* **1999**, *38*, 5154.

[49] V. Auger, T. Karantassis, *C. R. Hebd. Seances Acad. Sci.* **1925**, *181*, 665.

[50] S. J. Clark, J. D. Donaldson, J. A. Harvey, *J. Mater. Chem.* **1995**, *5*, 1813.

[51] G. Giorgi, K. Yamashita, *Chem. Lett.* **2015**, *44*, 826.

[52] a) A. H. Slavney, T. Hu, A. M. Lindenberg, H. I. Karunadasa, *J. Am. Chem. Soc.* **2016**, *138*, 2138; b) E. T. McClure, M. R. Ball, W. Windl, P. M. Woodward, *Chem. Mater.* **2016**, *28*, 1348; c) G. Volonakis, M. R. Filip, A. A. Haghighirad, N. Sakai, B. Wenger, H. J. Snaith, F. Giustino, *J. Phys. Chem. Lett.* **2016**, *7*, 1254.

[53] a) G. Volonakis, A. A. Haghighirad, R. L. Milot, W. H. Sio, M. R. Filip, B. Wenger, M. B. Johnston, L. M. Herz, H. J. Snaith, F. Giustino, *J. Phys. Chem. Lett.* **2017**, *8*, 772; b) J. Zhou, Z. Xia, M. S. Molokeev, X. Zhang, D. Peng, Q. Liu, *J. Mater. Chem. A* **2017**, *5*, 15031.

 © 2021 Wiley-VCH GmbH

These are not the final page numbers!

[54] A. H. Slavney, L. Leppert, A. Saldivar Valdes, D. Bartesaghi, T. J. Savenije, J. B. Neaton, H. I. Karunadasa, *Angew. Chem. Int. Ed.* **2018**, *57*, 12765; *Angew. Chem.* **2018**, *130*, 12947.

[55] T. T. Tran, J. R. Panella, J. R. Chamorro, J. R. Morey, T. M. McQueen, *Mater. Horiz.* **2017**, *4*, 688.

[56] Z. Deng, F. Wei, S. Sun, G. Kieslich, A. K. Cheetham, P. D. Bristowe, *J. Mater. Chem. A* **2016**, *4*, 12025.

[57] a) K.-z. Du, W. Meng, X. Wang, Y. Yan, D. B. Mitzi, *Angew. Chem. Int. Ed.* **2017**, *56*, 8158; *Angew. Chem.* **2017**, *129*, 8270; b) A. H. Slavney, L. Leppert, D. Bartesaghi, A. Gold-Parker, M. F. Toney, T. J. Savenije, J. B. Neaton, H. I. Karunadasa, *J. Am. Chem. Soc.* **2017**, *139*, 5015; c) K. P. Lindquist, S. A. Mack, A. H. Slavney, L. Leppert, A. Gold-Parker, J. F. Stebbins, A. Salleo, M. F. Toney, J. B. Neaton, H. I. Karunadasa, *Chem. Sci.* **2019**, *10*, 10620.

[58] V. Auger, T. Karantassis, *C. R. Hebd. Seances Acad. Sci.* **1925**, *180*, 1845.

[59] D. H. Brown, K. R. Dixon, D. W. A. Sharp, *J. Chem. Soc. A* **1966**, 1244.

[60] D. Sinram, C. Brendel, B. Krebs, *Inorg. Chim. Acta* **1982**, *64*, L131.

[61] a) N. Sakai, A. A. Haghighirad, M. R. Filip, P. K. Nayak, S. Nayak, A. Ramadan, Z. Wang, F. Giustino, H. J. Snaith, *J. Am. Chem. Soc.* **2017**, *139*, 6030; b) A. E. Maughan, A. M. Ganose, D. O. Scanlon, J. R. Neilson, *Chem. Mater.* **2019**, *31*, 1184; c) M.-G. Ju, M. Chen, Y. Zhou, H. F. Garces, J. Dai, L. Ma, N. P. Padture, X. C. Zeng, *ACS Energy Lett.* **2018**, *3*, 297.

[62] a) B. A. Connor, L. Leppert, M. D. Smith, J. B. Neaton, H. I. Karunadasa, *J. Am. Chem. Soc.* **2018**, *140*, 5235; b) B. A. Connor, R.-I. Biega, L. Leppert, H. I. Karunadasa, *Chem. Sci.* **2020**, *11*, 7708; c) L. Mao, S. M. L. Teicher, C. C. Stoumpos, R. M. Kennard, R. A. DeCrescent, G. Wu, J. A. Schuller, M. L. Chabinyc, A. K. Cheetham, R. Seshadri, *J. Am. Chem. Soc.* **2019**, *141*, 19099; d) L.-Y. Bi, Y.-Q. Hu, M.-Q. Li, T.-L. Hu, H.-L. Zhang, X.-T. Yin, W.-X. Que, M. S. Lassoued, Y.-Z. Zheng, *J. Mater. Chem. A* **2019**, *7*, 19662; e) M. K. Jana, S. M. Janke, D. J. Dirkes, S. Dovletgeldi, C. Liu, X. Qin, K. Gundogdu, W. You, V. Blum, D. B. Mitzi, *J. Am. Chem. Soc.* **2019**, *141*, 7955.

[63] a) B. Saparov, D. B. Mitzi, *Chem. Rev.* **2016**, *116*, 4558; b) M. D. Smith, B. A. Connor, H. I. Karunadasa, *Chem. Rev.* **2019**, *119*, 3104.

[64] J. Yang, P. Zhang, S.-H. Wei, *J. Phys. Chem. Lett.* **2018**, *9*, 31.

[65] Z. Xiao, W. Meng, J. Wang, Y. Yan, *ChemSusChem* **2016**, *9*, 2628.

[66] L. Schröder, H.-L. Keller, *Z. Anorg. Allg. Chem.* **1991**, *603*, 69.

[67] G. King, P. M. Woodward, *J. Mater. Chem.* **2010**, *20*, 5785.

[68] a) M. T. Anderson, K. R. Poeppelmeier, *Chem. Mater.* **1991**, *3*, 476; b) M. Azuma, S. Kaimori, M. Takano, *Chem. Mater.* **1998**, *10*, 3124.

[69] D. B. Mitzi, *J. Chem. Soc. Dalton Trans.* **2001**, 1.

[70] B. Vargas, E. Ramos, E. Pérez-Gutiérrez, J. C. Alonso, D. Solis-Ibarra, *J. Am. Chem. Soc.* **2017**, *139*, 9116.

[71] E. G. Tulsky, J. R. Long, *Chem. Mater.* **2001**, *13*, 1149.

[72] L.-Y. Bi, T.-L. Hu, M.-Q. Li, B.-K. Ling, M. S. Lassoued, Y.-Q. Hu, Z. Wu, G. Zhou, Y.-Z. Zheng, *J. Mater. Chem. A* **2020**, *8*, 7288.

[73] a) S. S. Nagapetyan, Y. I. Dolzhenko, E. R. Arakelova, V. M. Koshkin, Y. T. Struchkov, V. E. Shklover, *Zh. Neorg. Khim.* **1988**, *33*, 2806; b) J. Calabrese, N. L. Jones, R. L. Harlow, N. Herron, D. L. Thorn, Y. Wang, *J. Am. Chem. Soc.* **1991**, *113*, 2328; c) D. B. Mitzi, C. A. Feild, W. T. A. Harrison, A. M. Guloy, *Nature* **1994**, *369*, 467; d) I. C. Smith, E. T. Hoke, D. Solis-Ibarra, M. D. McGehee, H. I. Karunadasa, *Angew. Chem. Int. Ed.* **2014**, *53*, 11232; *Angew. Chem.* **2014**, *126*, 11414; e) C. M. M. Soe, G. P. Nagabhushana, R. Shivaramaiah, H. Tsai, W. Nie, J.-C. Blancon, F. Melkonyan, D. H. Cao, B. Traoré, L. Pedesseau, M. Kepenekian, C. Katan, J. Even, T. J. Marks, A. Navrotsky, A. D. Mohite, C. C. Stoumpos, M. G. Kanatzidis, *Proc. Natl. Acad. Sci. USA* **2019**, *116*, 58.

[74] E. T. McClure, A. P. McCormick, P. M. Woodward, *Inorg. Chem.* **2020**, *59*, 6010.

[75] a) E. R. Dohner, E. T. Hoke, H. I. Karunadasa, *J. Am. Chem. Soc.* **2014**, *136*, 1718; b) E. R. Dohner, A. Jaffe, L. R. Bradshaw, H. I. Karunadasa, *J. Am. Chem. Soc.* **2014**, *136*, 13154; c) M. D. Smith, H. I. Karunadasa, *Acc. Chem. Res.* **2018**, *51*, 619.

[76] a) R. Prasanna, A. Gold-Parker, T. Leijtens, B. Conings, A. Babayigit, H.-G. Boyen, M. F. Toney, M. D. McGehee, *J. Am. Chem. Soc.* **2017**, *139*, 11117; b) M. D. Smith, A. Jaffe, E. R. Dohner, A. M. Lindenberg, H. I. Karunadasa, *Chem. Sci.* **2017**, *8*, 4497.

[77] C. J. Howard, B. J. Kennedy, P. M. Woodward, *Acta Crystallogr. Sect. B* **2003**, *59*, 463.

[78] F. Wei, Z. Deng, S. Sun, F. Xie, G. Kieslich, D. M. Evans, M. A. Carpenter, P. D. Bristowe, A. K. Cheetham, *Mater. Horiz.* **2016**, *3*, 328.

[79] M. S. Wickleder, G. Meyer, *Z. Anorg. Allg. Chem.* **1995**, *621*, 457.

[80] F. C. Hawthorne, R. B. Ferguson, *Can. Mineral.* **1975**, *13*, 377.

[81] a) H. A. Evans, D. H. Fabini, J. L. Andrews, M. Koerner, M. B. Preefer, G. Wu, F. Wudl, A. K. Cheetham, R. Seshadri, *Inorg. Chem.* **2018**, *57*, 10375; b) P. Vishnoi, J. L. Zuo, T. A. Strom, G. Wu, S. D. Wilson, R. Seshadri, A. K. Cheetham, *Angew. Chem. Int. Ed.* **2020**, *59*, 8974; *Angew. Chem.* **2020**, *132*, 9059.

[82] a) C. E. Patrick, K. W. Jacobsen, K. S. Thygesen, *Phys. Rev. B* **2015**, *92*, 201205; b) A. Marronnier, H. Lee, B. Geffroy, J. Even, Y. Bonnassieux, G. Roma, *J. Phys. Chem. Lett.* **2017**, *8*, 2659; c) A. N. Beecher, O. E. Semonin, J. M. Skelton, J. M. Frost, M. W. Terban, H. Zhai, A. Alatas, J. S. Owen, A. Walsh, S. J. L. Billinge, *ACS Energy Lett.* **2016**, *1*, 880; d) K. T. Munson, J. R. Swartzfager, J. B. Asbury, *ACS Energy Lett.* **2019**, *4*, 1888.

[83] a) S. K. Jain, R. P. Goyal, B. R. K. Gupta, *Infrared Phys.* **1992**, *33*, 589; b) G. P. O'Leary, R. G. Wheeler, *Phys. Rev. B* **1970**, *1*, 4409; c) A. E. Maughan, A. M. Ganose, A. M. Candia, J. T. Granger, D. O. Scanlon, J. R. Neilson, *Chem. Mater.* **2018**, *30*, 472; d) U.-G. Jong, C.-J. Yu, Y.-H. Kye, S.-H. Choe, J.-S. Kim, Y.-G. Choe, *Phys. Rev. B* **2019**, *99*, 184105.

[84] A. E. Maughan, A. A. Paecklar, J. R. Neilson, *J. Mater. Chem. C* **2018**, *6*, 12095.

[85] Z. Xiao, K. Z. Du, W. Meng, D. B. Mitzi, Y. Yan, *Angew. Chem. Int. Ed.* **2017**, *56*, 12107; *Angew. Chem.* **2017**, *129*, 12275.

[86] R. Hoffmann, *Solids and Surfaces: A Chemist's View of Bonding in Extended Structures*, Wiley-VCH, Weinheim, **1988**.

[87] M. G. Goesten, R. Hoffmann, *J. Am. Chem. Soc.* **2018**, *140*, 12996.

[88] a) F. Brivio, K. T. Butler, A. Walsh, M. van Schilfgaarde, *Phys. Rev. B* **2014**, *89*, 155204; b) Y. Wang, T. Gould, J. F. Dobson, H. Zhang, H. Yang, X. Yao, H. Zhao, *Phys. Chem. Chem. Phys.* **2014**, *16*, 1424.

[89] B. Kang, K. Biswas, *J. Phys. Chem. C* **2016**, *120*, 12187.

[90] O. Laporte, *Z. Phys.* **1924**, *23*, 135.

[91] W. Meng, X. Wang, Z. Xiao, J. Wang, D. B. Mitzi, Y. Yan, *J. Phys. Chem. Lett.* **2017**, *8*, 2999.

[92] B. Saparov, J.-P. Sun, W. Meng, Z. Xiao, H.-S. Duan, O. Gunawan, D. Shin, I. G. Hill, Y. Yan, D. B. Mitzi, *Chem. Mater.* **2016**, *28*, 2315.

[93] M. Delor, A. H. Slavney, N. R. Wolf, M. R. Filip, J. B. Neaton, H. I. Karunadasa, N. S. Ginsberg, *ACS Energy Lett.* **2020**, *5*, 1337.

[94] a) A. Karmakar, M. S. Dodd, S. Agnihotri, E. Ravera, V. K. Michaelis, *Chem. Mater.* **2018**, *30*, 8280; b) N. K. Nandha, A. Nag, *Chem. Commun.* **2018**, *54*, 5205; c) J. D. Majher, M. B. Gray, T. A. Strom, P. M. Woodward, *Chem. Mater.* **2019**, *31*, 1738.

 © 2021 Wiley-VCH GmbH

[95] a) M. Osada, T. Sasaki, *Adv. Mater.* **2012**, *24*, 210; b) M. Xu, T. Liang, M. Shi, H. Chen, *Chem. Rev.* **2013**, *113*, 3766.
[96] a) J. Ihringer, S. C. Abrahams, *Phys. Rev. B* **1984**, *30*, 6540; b) G. P. Knudsen, *Solid State Commun.* **1984**, *49*, 1045.
[97] a) A. Kraft, *Bull. Hist. Chem.* **2008**, *33*, 61; b) A. Kraft in *Prussian Blue-Type Nanoparticles and Nanocomposites: Synthesis, Devices, and Applications*, 1 ed. (Eds.: Y. Guari, J. Larionova), Jenny Stanford Publishing, New York, **2019**, pp. 1 – 26.
[98] a) A. Ludi, H. U. Güdel in *Inorganic Chemistry. Structure and Bonding*, *Vol. 14*, Springer, Berlin, Heidelberg, **1973**, pp. 1 – 21; b) J. N. Behera, D. M. D′Alessandro, N. Soheilnia, J. R. Long, *Chem. Mater.* **2009**, *21*, 1922; c) M. Pyrasch, A. Toutianoush, W. Jin, J. Schnepf, B. Tieke, *Chem. Mater.* **2003**, *15*, 245.
[99] J. J. Alexander, H. B. Gray, *J. Am. Chem. Soc.* **1968**, *90*, 4260.
[100] a) K. A. Hofmann, F. Küspert, *Z. Anorg. Chem.* **1897**, *15*, 204; b) H. M. Powell, J. H. Rayner, *Nature* **1949**, *163*, 566; c) R. Baur, G. Schwarzenbach, *Helv. Chim. Acta* **1960**, *43*, 842; d) V. M. Bhatnagar, *J. Chem. Educ.* **1963**, *40*, 646.
[101] a) A. Splendiani, L. Sun, Y. Zhang, T. Li, J. Kim, C.-Y. Chim, G. Galli, F. Wang, *Nano Lett.* **2010**, *10*, 1271; b) K. F. Mak, C. Lee, J. Hone, J. Shan, T. F. Heinz, *Phys. Rev. Lett.* **2010**, *105*, 136805.
[102] D. Jariwala, V. K. Sangwan, L. J. Lauhon, T. J. Marks, M. C. Hersam, *ACS Nano* **2014**, *8*, 1102.
[103] D. A. Couch, C. J. Wilkins, G. R. Rossman, H. B. Gray, *J. Am. Chem. Soc.* **1970**, *92*, 307.
[104] E. M. Glebov, I. P. Pozdnyakov, V. F. Plyusnin, I. Khmelinskii, *J. Photochem. Photobiol. C* **2015**, *24*, 1.
[105] B. Schüpp, P. Heines, A. Savin, H. L. Keller, *Inorg. Chem.* **2000**, *39*, 732.
[106] L. R. Morss, W. R. Robinson, *Acta Crystallogr. Sect. B* **1972**, *28*, 653.
[107] Y. Xu, B. Jiao, T.-B. Song, C. C. Stoumpos, Y. He, I. Hadar, W. Lin, W. Jie, M. G. Kanatzidis, *ACS Photonics* **2019**, *6*, 196.

Manuscript received: December 5, 2020
Accepted manuscript online: February 23, 2021
Version of record online: ■■ ■■, ■■■■

 © 2021 Wiley-VCH GmbH
These are not the final page numbers!

Minireviews

Double Perovskites

N. R. Wolf, B. A. Connor, A. H. Slavney, H. I. Karunadasa* ——— ■■■■–■■■■

Doubling the Stakes: The Promise of Halide Double Perovskites

Two B sites in combination dictate the properties of halide double perovskites ($A_2BB'X_6$; A = monocation, X = halide). This Minireview gives a brief overview of the rich history of halide double perovskites, highlights key structural and electronic aspects, and describes the current understanding on how to correctly select the B-site pairs that afford the desired properties.

© 2021 Wiley-VCH GmbH